JOURNAL OF Applied Polymer SCIENCE

Frequency and voltage dependence of dielectric properties, complex electric modulus, and electrical conductivity in Au/7% graphene doped-PVA/n-Si (MPS) structures

Seçkin Altındal Yerişkin,[1] Muzaffer Balbaşı,[1] Adem Tataroğlu[2]
[1]Department of Chemical Engineering, Faculty of Engineering, Gazi University, Ankara, Turkey
[2]Department of Physics, Faculty of science and Arts, Gazi University, Ankara, Turkey
Correspondence to: M. Balbaşı (E-mail: mbalbasi@gazi.edu.tr)

ABSTRACT: In order to increase the capacitance of Au/n-Si (MS) structure, 7% graphene doped PVA was coated on n-Si as an interfacial layer. The measured data of capacitance (C) and conductance (G/ω) of Au/7% graphene doped-PVA/n-Si (MPS) structure was utilized for the calculation of real and imaginary parts of complex permittivity ($\varepsilon^* = \varepsilon' - j\varepsilon''$), loss tangent (tan$\delta$), complex electric modulus ($M^* = M' + jM''$), and electrical conductivity (σ). The admittance measurements (C and G/ω) were carried out in the frequency range of 0.5 kHz to 1 MHz at room temperature. Frequency dependence of the dielectric constant (ε'), dielectric loss (ε'') and tanδ shows a dispersive behavior at low frequencies. This behavior was explained by Maxwell–Wagner relaxation. Due to the dipolar and the interfacial polarizations, as well as the surface states (N_{ss}) and the interfacial PVA layer, the parameters exhibited a strong dependence on frequency and applied bias voltage. The σ versus log(f) plot exhibited both low and high frequency dispersion phenomena such that at low frequencies σ value corresponding to the dc conductivity (σ_{dc}), but at high frequencies it corresponds to the ac conductivity (σ_{ac}). M' and M'', both, have low values in the low frequency region. However, an increase is observed with the increasing frequency due to the short-range mobility of charge carriers. As a result, the change in dielectric parameters and electric modulus with frequency is the result of relaxation phenomena and surface states. © 2016 Wiley Periodicals, Inc. J. Appl. Polym. Sci. **2016**, *133*, 43827.

KEYWORDS: coatings; dielectric properties; electrospinning; films

Received 14 October 2015; accepted 25 April 2016
DOI: 10.1002/app.43827

INTRODUCTION

The surface stability of the semiconductors plays an important role in the fabrication of electronic devices such as the metal-insulator/oxide-semiconductor (MIS or MOS) and the metal–polymer-semiconductor (MPS) structures. Pure polymers are weak conductive materials. For this reason, metal doped polymers are examined as a potential material for replacing the traditional silicon-dioxide (SiO_2) interfacial layer between metal and semiconductor.[1–6] Among the various polymeric materials, poly(vinyl alcohol) (PVA) is a semi-crystalline and water-soluble polymer, nontoxic polymer and has low conductivity, wide range of crystallinity, very high dielectric strength, good charge storage capacity, interesting physical properties which arise from OH groups, and formation of hydrogen bonding.[7] For this respect, PVA is one of important polymeric materials which are utilized as interfacial organic material for the construction electronic devices. High conductivity, high dielectric constant and low dielectric loss can be obtained by doping appropriate metals or graphene into the PVA. In order to increase the capacitance [$C = \varepsilon'(\varepsilon_o A/d_i)$], it is important to increase the dielectric constant of interfacial layer (ε') and its thickness (d_i). In other words, high dielectric material is necessary to produce ultra/super capacitor and it can be used in a wide range of charge/energy storage applications.

Graphene exhibits several unique properties such as high carrier mobility, high mechanical strength, and high transparency in the visible range, tunable bandgap, high surface area ($\sim$2600 m^2/g).[8–10] Graphene was discovered by Geim's group in 2004 and since then, it has aroused tremendous scientific and industrial interest.[9] When graphene-doped polymer is used as interfacial layer between metal and semiconductor, the metal-semiconductor (MS) structure converts into MPS structure. As a result of this conversion, the MPS structure is able to store more electric charges in the form of a capacitor. Such high-κ interlayer does not only prevent inter-diffusion between metal and semiconductor, it also alleviates the electric field reduction

© 2016 Wiley Periodicals, Inc.

issue in MPS structure. Graphene has also a considerably high dielectric constant compared with conventional insulating materials and polymers and it is a new two-dimensional (2D) layer of sp^2 bonded carbon material, has emerged as a promising material in many fields owing to its extraordinary high specific surface area, excellent electric conductivity, and superior mechanical stability.[8] Graphene and GO are suitable to produce polymer composite materials. Both the physical and chemical properties of graphene/polymer composites depend on the nanofiller and polymer–matrix interface and dispersion amount. As far as we know, there is not any study in the literature on frequency and voltage dependence of dielectric properties, complex electric modulus and electrical conductivity of the Au/n-Si (MS) type structures with graphene-doped PVA interfacial layer in detail. Industrial graphene sources are in powder form or dispersion form, but it is too difficult to dissolve graphene any of the conventional solvents. Therefore, graphene is used as dispersion material. In order to overcome the issue about homogeneity, we used electrospinning technique instead of the other coating techniques. During the electrospinning process, graphene can be dispersed homogenously in polymeric material.

In this study, to determine the best doping concentration of graphene, MPS structure was fabricated with various graphene (0, 1, 3, 5, 7%) concentrations. Among them Au/(0.07 graphene doped PVA)/n-Si revealed the best physical characteristics. Therefore, we select the 7% graphene doped-PVA as interfacial layer between Au and n-Si semiconductor and coated it on n-Si using electrospinning method. Electrospinning process is a straight forward one that produces polymer nano-fabrics. When the electrical force applied, the force at surface of polymer solution overcomes the surface tension, a charged jet of polymeric solution is ejected and then the jet extends in a straight line for a certain distance. The electrospinning method also forms fabrics with diameters of one or two orders of magnitude smaller than those of conventional textile fabrics. The more information on electrospinning process and its advantages can be found in ref. 11 in detail.

In the ideal case, especially the capacitance value (MIS, MOS, and MPS type structures) usually considered independent from the frequency at high frequencies ($f \geq 500$ kHz) and the capacitance value increases with the increasing applied bias voltage. Contrary to the high frequencies, the capacitance values especially in depletion and accumulation regions at low and moderate frequencies become strongly dependent of frequency due to N_{ss}, surface charges, series resistance (R_s), interfacial layer, and its polarization.[12–14] It is well known that dielectric or polymeric materials can be polarized by applying an external electric field that displaces the charge carriers from their equilibrium position.[15] Dielectric permittivity of free dipoles oscillating in an alternating field can be described as follows: (a) at low angular frequencies (ω), period ($T = 1/2\pi f$) is higher than the inverse of relaxation time and dipoles can easy follow electrical field; (b) at moderate frequencies, as the frequency increases the dipoles begin to lag behind the a.c. signal of the field and ε' slightly decreases; (c) at the characteristic frequency where $\omega = 1/\tau$, ε' drops sharply (relaxation process); and (d) at quite high frequencies (T ` τ), the dipoles can no longer follow the field.[16–18] Electronic and atomic/ionic polarizations may occur only at very high frequencies ($\geq 10^{10}$ Hz)[19–23] whereas higher frequency value for our study is 10^6 Hz. On the other hand, dipolar/oriental polarization is effective in the frequency range of 1 kHz to 1 MHz, while interfacial polarization becomes effective in the low frequency region; below few kHz. According to thermionic emission (TE) theory, the value of barrier height (BH) between metal and semiconductor does not include the effect of applied bias voltage or electric field. However, in practice, the situation is considerably different from the ideal case. Therefore, the value of BH (Φ_b) should be replaced with the effective BH [$\Phi e = \Phi_b + (d\Phi e/dV)V$]. Here, ($d\Phi e/dV$) is the change in the BH with applied bias voltage. In MIS or MPS structures, potential "pinch off" frequently take place, leading to bias-dependent "saddle point" effective BH for any patch, with an effective conduction area that was applied bias voltage dependent.

As a result, studying the real and the imaginary parts of complex permittivity, complex electric modulus and electrical conductivity of the material is useful for the applications involving MOS and MPS type structures or capacitors. The aim of this study is fabricating Au/7% graphene doped-PVA/n-Si (MPS) structure and investigating its dielectric properties, electric modulus and conductivity as a function of frequency and bias voltage in detail. Thus it is shown that capacitance value of a MIS or MOS capacitor can be considerably increased by using such high-κ dielectric material, and so it can be used in a wide range of charge/energy storage applications.

EXPERIMENTAL DETAILS

Au/%7 graphene-doped PVA/n-Si (MPS) structures were fabricated by using n-Si wafer with the diameter of 5.08 cm, orientation of (100), thickness of 350 μm and Phosphor (dopant) atom concentration of 4.3×10^{15} cm^{-3}. At first step, wafer was dipped in ammonium peroxide for 40 s to remove native oxide layer on the surface and then in the next step, the wafer was etched in sequence with acid solutions (H_2SO_4:H_2O_2:H_2O = 3:1:1) for 60 s, and (HCl:H_2O = 1:1) for another 60 s. The cleaned wafer was rinsed with the deionized water having 18 MΩ resistivity. Subsequently, the wafer was dried by dry nitrogen (N_2) gas at room temperature. After the cleaning process, high purity Au (99.995%) with a thickness of approximately 1500 Å was thermally evaporated from the tungsten filament onto the back side of the n-Si wafer at a pressure of approximately 10^{-6} Torr in a high vacuum metal evaporation system. In order to perform the low resistivity ohmic back contact, Au coated n-Si wafer was sintered at 500 °C for 5 min in a nitrogen atmosphere.

After the formation of the ohmic contact, polyvinyl alcohol (PVA-Mw 130,000 g/mol, from Sigma Aldrich) was used as the polymeric precursor. Graphene powder was purchased from "Grafen Chemical Industries Co." Deionized water and acetic acid (100%, Merck) was used as a solvent. Graphene powder was added as preferably 7% of PVA powder. Firstly, the PVA solution (8% w/w) with deionized water was prepared by dissolving the PVA powder in ultrapure distilled and deionized

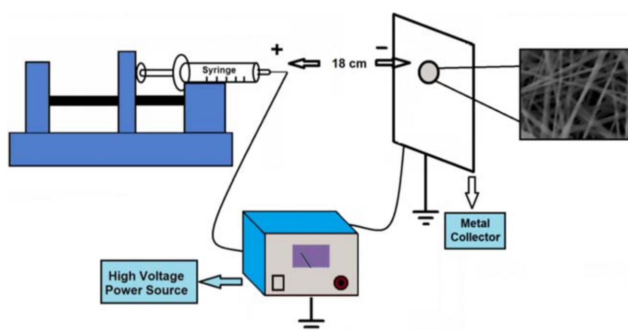

Figure 1. The schematic diagram of electrospinning system. [Color figure can be viewed in the online issue, which is available at wileyonlinelibrary.com.]

water while heating the solution at 80 °C and stirring for 3 h. Then the solution was cooled to the room temperature. Subsequently, the graphene solution (1.6% w/w) was prepared with N,N-dimethylformamide which is chosen as a solvent of this solution. The graphene solution (1.6% w/w) was placed in an Ultrasonic Shaker (Bandelin Sonorex, Berlin) for a 48-h period of time. After that, the PVA solution (8% w/w) and the graphene solution (1.6% w/w) were mixed at room temperature to produce a solution which will undergo the electro-spinning process. Lastly, the n-Si wafer was pasted upon metal collector and the solution of the PVA/graphene was coated on the wafer as nanosize fibers during 10 min via electro-spinning. The distance between the wafer and the syringe (polymer hybrid solution) was adjusted to 18 cm and a voltage of 17 kV was applied to the solution flowing at the rate of 0.5 mL/h. Thus polymeric nano-fibers were coated on the wafer. The electro-spinning system consisted of a direct current (DC) high-voltage power supply (Gamma High Voltage Research, Inc., Ormond Beach, FL; ES 30P-20 W/DAM), a dosing pump (New Era Syringe Pump), a plastic capillary tube (syringe), and a metal collector. The syringe was filled with polymer solutions before the copper pins were connected to the power supply.

Finally, the circular dots of 1 mm in diameter and 1500 Å in thickness of high purity Au rectifying contacts were deposited on the surface of polymeric layer through a metal shadow mask in the high vacuum system at about 10^{-6} Torr. Both Au ohmic and rectifier contacts were deposited at a rate of 4 Å/s through a metal shadow mask. Thus, the fabrication processes of Au/7% graphene-doped PVA/n-Si (MPS) structures were completed. The schematic diagram of electrospinning system and the schematic diagram of the fabricated samples are shown in Figures 1 and 2, respectively. For the admittance spectroscopy measurements, the samples were placed onto the Cu-holder using silver paste. In order to perform admittance measurements of fabricated samples, electrical connections were made by Ag coated thin copper wires with approximately 10 μm diameter. The admittance measurements of the fabricated samples were carried out in the frequency range of 0.5 kHz to 1 MHz at the room temperature by using an HP 4192A LF impedance analyzer. Small sinusoidal ac test signal with 40 mV from the external pulse generator is applied to the sample to meet the requirement. In order to eliminate the effects of environmental, moisture and noise, all measurements were carried out in the cryostat at 10^{-3} Torr and they were also recorded using an IEEE-488 data acquisition system incorporated into a personal computer. The experimental measurement system is given in Figure 3.

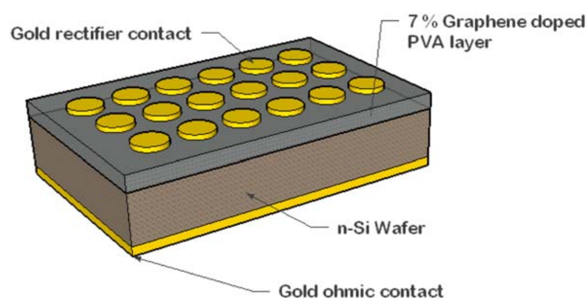

Figure 2. The schematic diagram of the Au/%7 graphene doped PVA/n-Si (MPS) structures. [Color figure can be viewed in the online issue, which is available at wileyonlinelibrary.com.]

RESULT AND DISCUSSIONS

In order to observe the dispersion of the real and imaginary parts of complex dielectric constant and electric modulus with frequency and applied bias voltage, *C–V* and *G*/ω*–V* measurements were carried out in the wide frequency range of 0.5 kHz to 1 MHz at room temperature. It is well known that the complex permittivity is expressed as $\varepsilon^* = \varepsilon' - i\varepsilon''$ where ε' is the real part and ε'' is the imaginary part. The voltage dependent ε' and ε'' values of the MIS, MOS, and MPS type structures were obtained from the measured capacitance (C_m) and conductance (G_m) values for each frequency by using following relations:

$$\varepsilon' = \frac{C_m}{C_i} = \frac{C_m d_i}{\varepsilon_o A} \quad (1)$$

$$\varepsilon'' = \frac{G_m}{\omega\ C_i} = \frac{G_m d_i}{\varepsilon_o \omega A} \quad (2)$$

where, C_i ($=\varepsilon_o A/d_i$) is the capacitance of empty capacitor with ε_o ($=8.85\times10^{-14}$ F/cm) is the permittivity of free space, $\omega(=2\pi f)$ is the angular frequency with the frequency of applied field, d_i (404 nm) is the thickness of interfacial layer and A is the

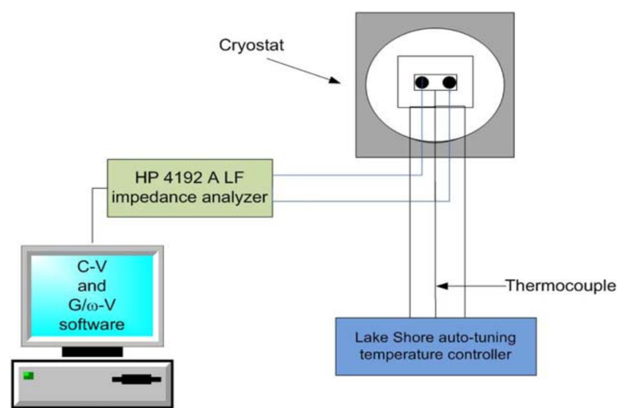

Figure 3. Experimental measurement system of *C–V* and *G*/ω*–V*. [Color figure can be viewed in the online issue, which is available at wileyonlinelibrary.com.]

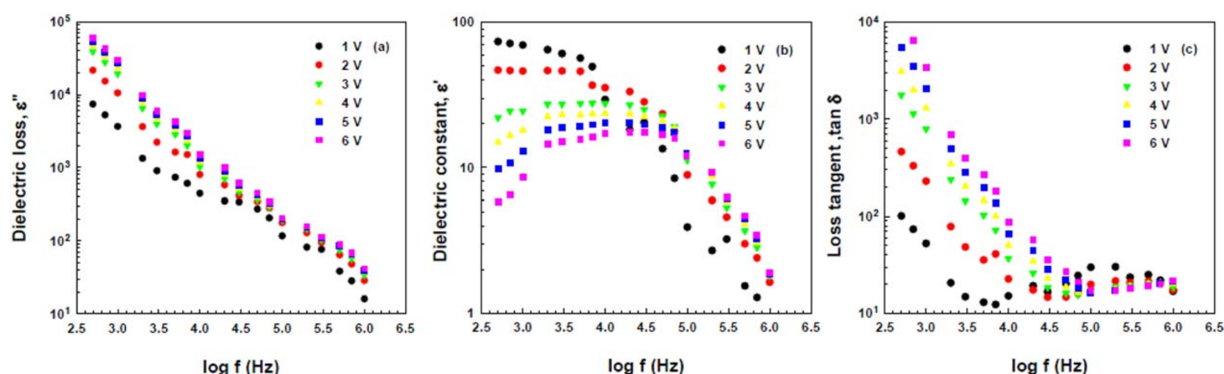

Figure 4. Frequency dependent (**a**) ε′, (**b**) ε″, and (**c**) tanδ characteristics of the Au/%7 graphene doped PVA/n-Si (MPS) structure for various applied bias voltages. [Color figure can be viewed in the online issue, which is available at wileyonlinelibrary.com.]

rectifier contact area. In addition, the real value of ε′ was obtained from the measured maximum capacitance value of the structure at strong accumulation region which is related to the interfacial layer capacitance ($C_a=C_i=\varepsilon'\varepsilon_o A/d_i$). The tangent (tanδ) is the ratio of energy dissipated per radian in the dielectric material (ε″) to the energy stored at the peak of polarization (ε′). Therefore, the investigation of tanδ as a function of frequency and voltage is an important subject. The value of dielectric loss tangent determines the conduction mechanism and the dielectric relaxation and it was calculated using the obtained ε′ and ε″ values in the equation below.

$$\tan\delta=\frac{\varepsilon''}{\varepsilon'} \tag{3}$$

The frequency dependent ε′, ε″, and tanδ values of the Au/7% graphene doped-PVA/n-Si (MPS) structure in the frequency range of 0.5 kHz to 1 MHz were determined using eqs. (1–3) at room temperature, respectively. Usually, the change in the conductivity is a result of restructuring and reordering of charges at the graphene-doped PVA/n-Si interface under external electric field or voltage and interface polarization. In this way, ε′, ε″, and tanδ values versus frequency plots were drawn and represented in Figure 4(a–c) for various forward applied bias voltages in the double-logarithmic scale, respectively.

As seen in Figure 4, the values of ε′, ε″, and tanδ are strongly dependent on frequency and they usually decrease with increasing frequency. The changes in these parameters become considerably high especially at low and intermediate frequencies. Such decrease in the ε′, ε″, and tanδ values with increasing frequency indicates that the interfacial dipoles have less time to orient themselves in the direction of the alternating electric field as the frequency is increased.[24–26] It can be said that at high frequencies, the value of dielectric constant decreases due to the shorter time available for the dipoles to align.[27] At low and intermediate frequencies, dipoles in the dielectric or polymeric material can easily be polarized under an external applied bias voltage or an electric field that displaces the charges from their equilibrium position or traps. In other words, the changes in the dielectric parameters with the frequency are the result of the relaxation time. The experimental results of this study confirmed that both dipole and interfacial polarizations can easily occur at low frequencies and additional charges at traps can easily follow the ac signal. Therefore, in the high frequency range, dielectric constant becomes saturated or independent of frequency.

One important effect on the electric and dielectric parameter is the charges at surface states/interface traps which are located between interfacial layer and semiconductor. Because of the surface states and bulk traps where charges can be stored and released when the appropriate forward applied bias and the external ac alternating voltage are applied, a charge effect can be produced on the devices.[12,13,28–30]

When the frequency is sufficiently low, the surface states can follow the ac signal and yield an excess capacitance ($C_{ex.}$) and conductance ($G_{ex.}/\omega$), which depends on their relaxation time and the frequency of the ac signal. When the capacitance and conductance measurements are held at the sufficiently high frequencies, the surface states cannot contribute to the C and G values. Although, it is believed that the injection of charge carriers involves a process of hopping to localized interface states, detailed physical mechanisms have not been well understood yet. The R_s of the device can also cause a serious error in the extraction of dielectric properties. While R_s is effective only in the accumulation region, N_{ss} is effective in the inversion and depletion regions, both. The variation of the values of ε′ and ε ″ with frequency indicates a normal dielectric dispersion due to Maxwell–Wagner[31] and space charge polarization.[32] The Maxwell–Wagner relaxation mechanism is associated with the uncompensated surface charges at interface inside the capacitors.[33] In order to study the effect of applied bias voltage on the frequency dependent ε′ and ε″ values, the various different forward applied bias voltages (1, 3, and 6 V) are represented in Figure 5(a–c).

As can be seen in Figure 4(a), obtained values of dielectric constant (ε′) for 7% graphene doped-PVA even at 0.5 kHz is almost 26 times greater than those of conventional SiO_2 and 3 times greater than high-dielectric TiO_2 interfacial layer. In this way, it is shown that by using high dielectric material, the value of capacitance of MIS or MOS capacitor can be increased considerably and it can be used in a wide range of charge/energy storage applications. Moreover, such high dielectric interlayer does not only prevent inter-diffusion between metal and semiconductor, but also alleviates the electric field reduction issue in these structures.

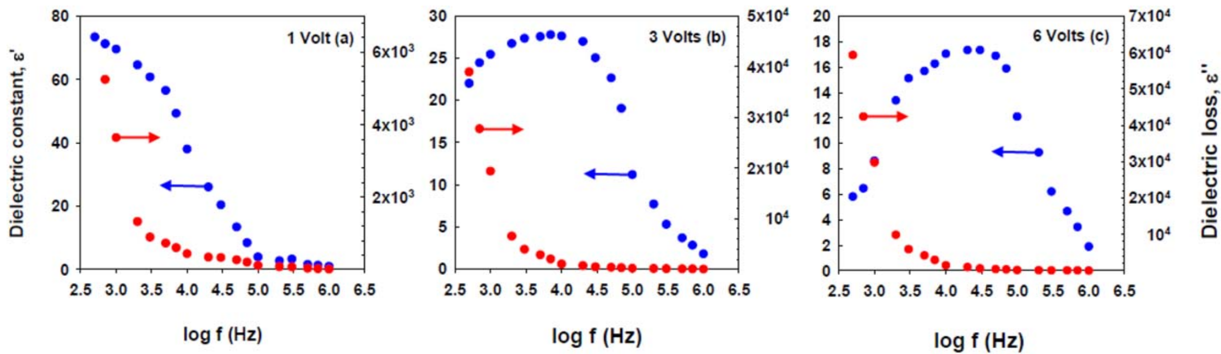

Figure 5. The changes in ε′ and ε″ of the Au/%7 graphene-doped PVA/n-Si (MPS) structure with frequency at bias voltages of (**a**) 1 V, (**b**) 3 V, and (**c**) 6 V. [Color figure can be viewed in the online issue, which is available at wileyonlinelibrary.com.]

As illustrated in Figure 5(a), for the low forward biases (1 V), ε′ and ε″ values decrease with increasing frequency, but there is a discrepancy between 1 and 100 kHz due to the dipole and surface polarizations and N_{ss}.[16] Because at high frequencies the surface states located between interfacial insulator layer and semiconductor cannot follow the ac signal, the value of ε′ becomes closer to the value of ε″ values. Contrary to low forward biases, the ε′ and ε″ versus the log*f* plots show an intersection behavior for sufficiently high forward biases ($V \geq 3$ V). As can be seen in Figure 5(b,c), at the low frequencies ($f \leq 10$ kHz), ε′ increases with increasing frequency, while ε″ decreases. It is evident that the minimum value of ε′ at about 10 kHz corresponds to the maximum value of the ε″ due to inductive behavior of the structure. Inductive behavior was attributed to the relaxation-like nature of the material due to the injection of holes which recombine easily with the electron free carriers of the dipole near the junction and hence decrease the charge dipole. According to Jones *et al.*[34] inductive behavior stems from the relaxation-like nature of the material due to injection of holes which recombine easily with the electron free carriers of the dipole near the junction and hence decrease the charge dipole. On the other hand, Champness *et al.*[35] ascribed the term of inductive behavior such that the material displays an inductive behavior due to the injection of minority carriers at forward applied bias voltage. According to us, such inductive behavior at low and intermediate frequencies for high voltage is the results of surface states, surface polarization, and series resistance.

In order to explain the dielectric relaxation of the dielectric materials, the complex electric modulus (M^*) formalisms is also used quite often.[35–38] The complex permittivity data are transformed into the M^* formalism using the following equation[38–40]:

$$M^* = \frac{1}{\varepsilon^*} = M' + jM'' = \frac{\varepsilon'}{\varepsilon'^2 + \varepsilon''^2} + j\frac{\varepsilon''}{\varepsilon'^2 + \varepsilon''^2} \qquad (4)$$

where, *j* is the imaginary root of (−1), *M*' and *M*″ are the real and imaginary parts of M^*, respectively. Figure 6(a,b) shows the double logarithmic *M*′–*f* and *M*″–*f* plots of the MPS structure for various forward bias voltages, respectively. As can be seen in Figure 6, *M*′ and *M*″, both, increase with increasing frequency. Such behavior in *M*′ and *M*″ with frequency can be attributed to the polarization.[38–40] However, the value reaches a maximum at high frequencies for each applied forward bias voltage corresponding to $M_\infty = 1/\varepsilon'_\infty$, due to relaxation processes.[39–45] In other words, both *M*' and *M*″ approach almost to zero at low frequencies.

As mentioned previously, a charge effect can be produced on the devices due to the surface states and bulk traps where charges can be stored and released when the appropriate forward applied bias and the external ac alternating voltage are applied.[12,13,28–30] As a result, it can be said that the peak behavior in *M* and tanδ, both, or the change in them with frequency indicates that the structure exhibits relaxation phenomena.[15,16,46,47] Moreover, especially in

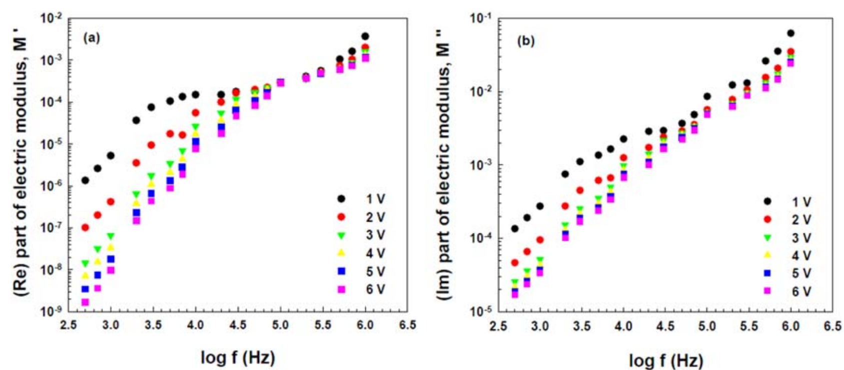

Figure 6. Frequency dependent (**a**) *M*′ and (**b**) *M*″ characteristics of the Au/%7 graphene doped PVA/n-Si (MPS) structure for various applied bias voltages. [Color figure can be viewed in the online issue, which is available at wileyonlinelibrary.com.]

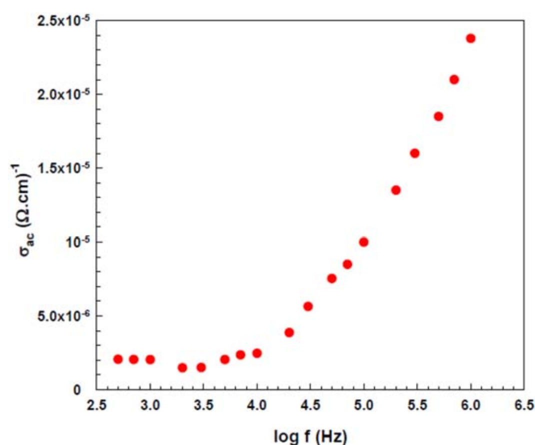

Figure 7. Frequency dependent total electrical conductivity (σ) of the Au/%7 graphene doped PVA/n-Si (MPS) structure for 1 V. [Color figure can be viewed in the online issue, which is available at wileyonlinelibrary.com.]

narrow-forbidden bandgap semiconductor, the charge carriers are not sufficiently free to move, but they can be trapped and so this causes a polarization.[44] On the other hand, as can be seen in Figure 4(a), the value of ε' starts to decrease rapidly at high frequencies since space charge polarization weakens.

In addition, as can be seen in Figure 6(a), the value of M' increases rapidly with increasing frequency due to the short range mobility of charge carriers and it can be attributed to the lack of a restoring force for flow of charges under the influence of a steady electric field.[35,36] The asymmetric modulus behavior which is shifted toward the high frequency side with a rise in applied bias voltage and exhibit the correlation between the motions of mobile charge carriers.[35–38] In addition, the hopping of carriers between surface states may be dominated in conduction mechanism.[47] In other words, the conductivity may be treated as electric field-activated hopping from traps to traps.

The frequency-dependent total electrical conductivity (σ) of the MPS structure was also obtained from the following equation[40–44] for 1 V at room temperature and it is shown in Figure 7.

$$\sigma(\omega)=\left(\frac{d}{A}\right)\omega C\tan\delta=\varepsilon''\omega\varepsilon_0=\sigma_{dc}+A\omega^n \tag{5}$$

where, σ_{dc} is the dc conductivity corresponding to low frequencies, σ_{ac} is the ac conductivity corresponding to the high frequencies (Figure 7), A is a constant of proportionality depended on frequency, and ω is angular frequency ($=2\pi f$ or $2\pi/T$).

The value of n in eq. (5) changes between 0 and 1. The semi-logarithmic σ versus f plot at 1 V has two different regions and it is evident that there exist two different conduction mechanisms which correspond to the low and high frequency regions. As shown in Figure 7, the value of σ_{ac} increases with increasing frequency in the frequency range of 10 kHz to 1 MHz, while the values of σ_{dc} becomes almost constant in the frequency range of 0.5–10 kHz. As the frequency increases, σ_{ac} increases because the polarization decreases with increasing frequency. The increase in the σ_{ac} also leads to an increase in the eddy current which in turn increases the energy loss tanδ. On the other hand, the hopping of carries from surface states to other N_{ss} located in the forbidden band gap of the semiconductor leads to an increase in frequency dependent electrical conductivity.[37,45–47]

CONCLUSIONS

The admittance spectroscopy measurements (C–V and G/ω–V) of the fabricated Au/%7 graphene doped PVA/n-Si (MPS) structure were carried out in the wide frequency range of 0.5 kHz to 1 MHz at room temperature for the purpose of obtaining more information on the dielectric properties, electric modulus and electrical conductivity. Experimental results confirmed that the dispersion in ε', ε'', tanδ, M', M'', and σ_{ac} values of the MPS structure are considerably high especially at the low frequencies due to the dipole and the surface polarizations and the N_{ss}. The frequency dependence of ε', ε'', and tanδ exhibit a dispersive behavior at low frequencies and this was explained on the basis of the Maxwell–Wagner relaxation. The decrease in the ε', ε'', and tanδ values with increasing frequency showed that the interfacial dipoles have less time to orient themselves in the direction of the alternating of the electric field as the frequency is increased. In other words, at low and intermediate frequencies, the dielectric or polymeric material can be easily polarized under an external applied bias voltage or electric field that displaces the charges from their equilibrium position or traps. These results confirmed that dipole and interfacial polarizations, both, can easily occur in the low frequency region and the additional charges at traps can easily follow the ac signal. Semi-logarithmic ε'–f and ε''–f plots at various applied bias voltages were investigated in order to assess the effect of applied bias voltage on ε' and ε''. Contrary to low forward biases, semi-logarithmic ε'–f and ε''–f plots show an intersection behavior for sufficiently high forward biases ($V \geq 3$ V). In other words, the minimum value of ε' at about 10 kHz corresponds to the maximum value of the ε'' due to inductive behavior of the structure. Inductive behavior was attributed to the relaxation-like nature of the material due to the injection of holes which recombine easily with the electron free carriers of the dipole near the junction and hence decrease the charge dipole. Surface states, the surface polarization and the R_s are also the others sources of inductive behavior of the Au/7% graphene doped-PVA/n-Si (MPS) structure. The values of M' and M'', both, were considerably low in the low frequency region and then they begin to increase with increasing frequency due to the increasing polarization in the Au/%7 graphene doped PVA/n-Si (MPS) structure with increasing frequency. The value of M' reaches a maximum value at high frequencies for each applied bias voltage, corresponding to $M_\infty = 1/\varepsilon_\infty$, due to relaxation processes. As a result, in the high frequency range, dielectric constant becomes saturated or independent of frequency. The σ versus log$f$ plot for sufficiently high voltages exhibited both low and high frequency dispersion phenomena such that at low frequencies σ value corresponding to the dc conductivity (σ_{dc}), but at high frequencies it corresponds to the ac conductivity (σ_{ac}). In conclusion, the change in dielectric parameters and electric modulus with frequency is the result of relaxation phenomena and surface states.

REFERENCES

1. Shash, N. M.; Khoder, H.; Metawa, F.; Negm, A. A. *J. Appl. Polym. Sci.* **2013**, *129*, 2796.
2. Barış, B. *Phys. E* **2013**, *54*, 171.
3. Kaya, A.; Vural, Ö.; Tecimer, H.; Demirezen, S.; Altındal, Ş. *Curr. Appl. Phys.* **2014**, *14*, 322.
4. Dökme, İ.; Tunç, T.; Uslu, İ.; Altındal, S. *Synth. Met.* **2011**, *161*, 474.
5. Demirezen, S.; Sönmez, Z.; Aydemir, U.; Altındal, Ş. *Curr. Appl. Phys.* **2012**, *12*, 266.
6. Shuyin, S.; Guilling, S.; Xiangyu, C.; Linna, Z.; Fanggao, C. *Compos. Sci. Technol.* **2014**, *97*, 115.
7. Mott, N. F.; Davis, E. A. Electronic Processes in Non-Crystalline Materials; Clarendon Press: Oxford, **1971**.
8. Li, H.; Jiao, W.; Yanan, O.; Jianling, Z.; Jian, Y.; Guosheng, W. *Colloids Surf. A: Physiochem. Eng. Aspects* **2014**, *449*, 148.
9. Novoselov, K. S.; Geim, A. K.; Morozov, S. V.; Jiang, D.; Zhang, Y.; Dubonos, S. V. *Science* **2004**, *306*, 666.
10. Dongrui, W.; Xiaoman, Z.; Jun-Wei, Z.; Jun, Z.; Zhi-Min, D.; Guo-Hua, H. *Polymer* **2013**, *54*, 1916.
11. Lee, J. S.; Choi, K. H.; Ghim, H. D.; Kim, S. S.; Chun, D. H.; Kim, H. Y.; Lyoo, W. S. *J. Appl. Polym. Sci.* **2004**, *93*, 1638.
12. Nicollian, E. H.; Brews, J. R. Metal Oxide Semiconductor (MOS) Physics and Technology; John Willey & Sons: New York, **1982**.
13. Sze, S. M. Physics of Semiconductor Devices, 2nd ed.; Wiley: New York, **1981**.
14. Card, H. C.; Rhoderick, E. H. *J. Phys. D-Appl. Phys.* **1971**, *4*, 1589.
15. Ishai, B. P.; Sader, E.; Felner, Y.; Weger, M. *J. Supercond.* **2005**, *18*, 455.
16. Dutta, A.; Bharti, C.; Sinha, T. P. *Mater. Res. Bull.* **2008**, *43*, 1246.
17. Hoque, Md. M.; Dutta, A.; Kumar, S.; Sinha, T. P. *Phys. B* **2012**, *407*, 3740.
18. Hoque, Md. M.; Dutta, A.; Kumar, S.; Sinha, T. P. *J. Mater Sci. Technol.* **2014**, *30*, 311.
19. Hench, L. L.; West, J. L. Principles of Electronic Ceramics; Wiley: New York, **1990**.
20. Kaplan, I. G.; Soullard, J.; Hernandez-Cobos, J. *Phys. Rev. B* **2002**, *65*, 214509.
21. Fuzukumi, Y.; Mizuhashi, K.; Ushida, S. *Phys. Rev. Lett.* **1996**, *76*, 684
22. Viera, V. N.; Pureur, P.; Schaf, J. *Phys. Rev. B* **2002**, *66*, 224506.
23. Rahim, M.; Khan, N. A.; Mumtaz, M. *J. Low. Temp. Phys.* **2013**, *172*, 47
24. Ho, J.; Jow, T. C.; Boggs, S. *IEEE Electr. Insul. Mag.* **2010**, *26*, 19.
25. Büyükbaş, A.; Tataroğlu, A.; Balbaşı, M. *J. Optoelectron. Adv. Mater.* **2015**, *17*, 1134.
26. Lin, J. H.; Zeng, J. J.; Lin, Y. J. *Thin Solid Films* **2014**, *550*, 582.
27. Chandrakala, H. N.; Shivakumaraiah, B. R.; Madhu Siddaramaiah, G. M. *J. Mater. Sci.* **2012**, *47*, 8076.
28. Bisquert, J.; Garcia-Belmonte, G.; Pitarch, A.; Bolink, H. J. *Phys. Lett.* **2006**, *422*, 184.
29. Tataroğlu, A.; Altındal, Ş. *Microelectron. Eng.* **2008**, *85*, 1866.
30. Noor Mohammad, S.; Fan, Z. F.; Botchkarev, A. E.; Kim, W.; Aktas, O.; Markoç, H.; Shiwei, F.; Jones, K. A.; Derenge, M. A. *Philos. Mag. B* **2001**, *81*, 453.
31. Wagner, K. W. *Ann. Phys.* **1913**, *40*, 817.
32. Bidault, O.; Goux, P.; Kchikech, M.; Belkaoumi, M.; Maglione, M. *Phys. Rev. B* **1994**, *49*, 7868.
33. Gorodea, I.; Goanta, M.; Toma, M. *J. Alloys Compd.* **2015**, *632*, 805.
34. Jones, B. K.; Santana, J.; McPherson, M. *Solid State Commun.* **1998**, *107*, 47.
35. Pissis, P.; Kyritsis, A. *Solid State Ion* **1997**, *97*, 105.
36. Champness, C. H.; Clark, W. R. *Appl. Phys. Rev. Lett.* **1990**, *56*, 1104.
37. Prabakar, K.; Narayandass, S. K.; Mangalaraj, D. *Phys. Stat. Sol.* **2003**, *199*, 507.
38. Macedo, P. B.; Moyniham, C. T.; Bose, R. *Phys. Chem. Glasses* **1972**, *13*, 171.
39. Afandiyeva, İ.; Bülbül, M. M.; Altındal, Ş.; Bengi, S. *Microelectron. Eng.* **2012**, *93*, 50.
40. Tripathi, S. K.; Sharma, M. *J. Appl. Phys.* **2012**, *111*, 074513.
41. Altındal Yerişkin, S.; Ünal, H. I.; Sarı, B. *J. Appl. Polym. Sci.* **2011**, *120*, 390.
42. Şafak Asar, H. Y.; Asar, T.; Altındal, Ş.; Özçelik, S. *J. Alloys Compd.* **2015**, *628*, 442.
43. Tataroğlu, A. *Microelectron. Eng.* **2006**, *83*, 2551.
44. Çetinkaya, H. G.; Alialy, S.; Altındal, Ş.; Kaya, A.; Uslu, İ. *J. Mater. Sci: Mater. Electron.* **2015**, *26*, 3186.
45. Chelkowski, A. Dielectric Physics; Elsevier: Amsterdam, **1980**.
46. Kaya, A.; Alialy, S.; Demirezen, S.; Balbaşı, M.; Yerişkin, S. A.; Aytemur, A. *Ceram. Int.* **2016**, *42*, 3322.
47. Altındal, S.; Sarı, B.; Ünal, H. I.; Yavaş, N. *J. Appl. Polym. Sci.* **2009**, *1113*, 2955.